

# Monte Carlo renormalization group study of the Heisenberg and the XY antiferromagnet on the stacked triangular lattice and the chiral $\phi^4$ model

M. Itakura

*JST, Center for Promotion of Computational Science and Engineering, Japan Atomic Energy Research Institute, Meguro-ku, Nakameguro 2-2-54, Tokyo 153, Japan*

(December 2, 2024)

With the help of the improved Monte Carlo renormalization-group scheme, we numerically investigate the renormalization group flow of the antiferromagnetic Heisenberg and XY spin model on the stacked triangular lattice (STA-model) and its effective Hamiltonian,  $2N$ -component chiral  $\phi^4$  model which is used in the field-theoretical studies. We find that the XY-STA model with the lattice size  $L = 96$  exhibits clear first-order behavior. We also find that the renormalization-group flow of STA model is well reproduced by the chiral  $\phi^4$  model, and that there are no chiral fixed point of renormalization-group flow for  $N = 2$  and 3 cases, indicating that the Heisenberg-STA model also undergoes first-order transition.

PACS numbers: 75.10.Nr

## I. INTRODUCTION

The critical behavior of the antiferromagnetic vector spin models on the stacked triangular lattice (STA) is still a controversial issue even after twenty years of extensive studies by means of experimental, field-theoretical, and numerical methods. See<sup>1–5</sup> for recent works, and<sup>6</sup> for a review.

The field-theoretical renormalization group (RG) analysis tells that when the number of spin component  $N$  is greater than some threshold value  $N_c$ , there are so-called "chiral fixed point" of RG which controls the critical behavior of the model and is characterized by novel values of critical exponents, while for  $N < N_c$  such fixed point disappears and the phase transition is of first order (see<sup>6</sup> for a review). Theoretical estimations of  $N_c$  have been made by various authors by means of  $\epsilon$ -expansion<sup>2,7,8</sup>, fixed dimensional perturbation<sup>2,3,9</sup>, local potential approximation<sup>10</sup>, and effective average action approach<sup>1</sup>, but the estimated values ranges from negative value to 6.5, depending on the method employed (however, recent results tend to be around 6.0). Thus the critical behavior of the physical relevant cases  $N = 2$  (XY spin) and  $N = 3$  (Heisenberg spin) is still unclear. A number of experimental studies<sup>4</sup> and numerical simulations<sup>11,12</sup> have yielded results which suggest second-order phase transition for  $N = 2$  and 3. However, recently it has been pointed out that the critical exponent  $\eta$  calculated from scaling relation becomes negative in some of these results, which is unphysical and indicates that the observed critical behavior is in fact pseudo-critical behavior induced by the slow RG flow<sup>1,5,10</sup>.

The present work intends to clarify the issue by numerically observing the RG flow and investigating whether there are chiral fixed point or not for several values of  $N$ . The paper

is organized as follows. In the next section, we will present the method by which we observe the RG flow in the Monte Carlo simulations. Details of the Monte Carlo simulations are given in Sec. III. In Sec. IV the RG flow obtained from the simulations for  $N = 2, 3, 8$  cases are presented. The last section is devoted to the concluding remarks.

## II. NUMERICAL OBSERVATION OF THE RG FLOW

### A. chiral $\phi^4$ model

The critical behavior of the  $N$ -component STA models are essentially described by the following  $2N$ -component Ginzburg-Landau-Wilson Hamiltonian<sup>6</sup>:

$$H = \int dx \left[ K \left( (\nabla \vec{\phi}_a)^2 + (\nabla \vec{\phi}_b)^2 \right) + r \left( \vec{\phi}_a^2 + \vec{\phi}_b^2 \right) + u \left( \vec{\phi}_a^2 + \vec{\phi}_b^2 \right)^2 + v \left( (\vec{\phi}_a \cdot \vec{\phi}_b)^2 - \vec{\phi}_a^2 \vec{\phi}_b^2 \right) \right], \quad (1)$$

where  $\vec{\phi}_a$  and  $\vec{\phi}_b$  are  $N$ -component vector defined on the continuum space. In the field-theoretical studies,  $K$  is fixed to unity to eliminate ambiguity of coefficients induced by a trivial rescaling of  $\phi$ , namely,  $\vec{\phi} \rightarrow c\vec{\phi}$ . In this regularization scheme,  $r$  plays a role of temperature. In the present work we concentrate on the case  $v \geq 0$ . The renormalization group flow of  $r$ ,  $u$ , and  $v$  becomes the one shown in Fig. 1. Above the critical plane, the flow is attracted to the high-temperature fixed point  $(r, u, v) = (\infty, 0, 0)$ . Below the critical plane, if  $v > 0$ , the flow is attracted to the anisotropic low-temperature fixed point  $(-\infty, \infty, \infty)$ , while on the isotropic plane  $v = 0$ , the flow is attracted to the isotropic low-temperature fixed point  $(-\infty, \infty, 0)$ . The flow on the critical plane projected onto the  $u$ - $v$  plane is shown in Fig. 2 for (a)  $N < N_c$  and (b)  $N > N_c$  cases. When  $N > N_c$ , there are stable and unstable chiral fixed points denoted by  $C_1$  and  $C_2$ , respectively, beside the  $O(2N)$  symmetric and the Gaussian fixed points denoted by O and G, respectively. The two fixed points  $C_1$  and  $C_2$  approach as  $N$  decreases, and annihilate each other at  $N = N_c$ .

To observe the RG flow directly from the numerical simulation, we use the lattice version of the Hamiltonian (1):

$$H = \frac{K}{2} \sum_{\langle ij \rangle} (\vec{\phi}(i) - \vec{\phi}(j))^2 + r \sum_i \vec{\phi}(i)^2 + u \sum_i \left( \vec{\phi}(i)^2 \right)^2 + v \sum_i \left[ (\vec{\phi}_a(i) \cdot \vec{\phi}_b(i))^2 - \vec{\phi}_a(i)^2 \vec{\phi}_b(i)^2 \right], \quad (2)$$

where  $\vec{\phi}(i) = (\vec{\phi}_a(i), \vec{\phi}_b(i))$  is an  $N + N$ -component vector defined on a lattice site  $i$  of  $L \times L \times L$  cubic lattice with periodic boundary condition being imposed, the summation  $\sum_{\langle ij \rangle}$  runs over all nearest neighbor pairs of the lattice site.

In the numerical simulations, we use a restriction  $u + v/4 - 2r = 0$  so that the minimum of the Hamiltonian takes place at  $|\vec{\phi}(i)| = 1$ , which removes the ambiguity of the trivial rescaling of  $\phi$ . Actually we use the following parameterization:

$$r = -2\lambda, \quad u = \lambda(1 + A), \quad v = 4\lambda A \quad (3)$$

where  $A$  controls the strength of the anisotropy and  $\lambda$  controls the "hardness" of the spin—the larger  $\lambda$  is, the smaller the fluctuation of  $|\vec{\phi}(i)|$  is. Then we observe the following quantities in Monte Carlo simulations:

$$C_L = \frac{\langle \vec{M}(\mathbf{k}_1) \cdot \vec{M}(-\mathbf{k}_1) \rangle}{\langle \vec{M}^2 \rangle}, \quad (4)$$

$$U_L = \frac{\langle (\vec{M}^2)^2 \rangle}{\langle \vec{M}^2 \rangle^2}, \quad (5)$$

$$V_L = \frac{\langle \vec{M}_a^2 \vec{M}_b^2 - (\vec{M}_a \cdot \vec{M}_b)^2 \rangle}{\langle \vec{M}^2 \rangle^2}, \quad (6)$$

where  $\vec{M}_a = \sum_i \vec{\phi}_a(i)$ ,  $\vec{M}_b = \sum_i \vec{\phi}_b(i)$ ,  $\vec{M} = \sum_i \vec{\phi}(i)$ ,  $\vec{M}(\mathbf{k}_1) = \sum_{\mathbf{r}} \exp(i\mathbf{k}_1 \cdot \mathbf{r})$  with  $\mathbf{k}_1 = (2\pi/L, 0, 0)$ , and the symbol  $\langle \rangle$  denotes thermal average in the  $L \times L \times L$  lattice.  $C_L$ ,  $U_L$  and  $V_L$  are thermal averages of the first, third, and fourth term, respectively, of (2) in the renormalized Hamiltonian<sup>13</sup>.

If one plot  $(U_L, V_L, C_L)$  for fixed values of  $A$ ,  $\lambda$ ,  $K$  and increasing values of  $L$ , the point moves along the arrows shown in Fig. 3. A number of trivial fixed points, namely, high-temperature fixed point  $(1 + 1/2N, \frac{(2N+1)(N-1)}{8N(N+1)}, 1)$ , isotropic low-temperature fixed point  $(1, \frac{N-1}{4(N+1)}, 0)$ , and anisotropic low-temperature fixed point  $(1, \frac{1}{4}, 0)$  are denoted by H,  $L_0$ , and  $L_1$ , respectively. If the probability distribution of the order parameter  $\vec{M}$  is isotropic, a relation  $V_L = \frac{N-1}{4(N+1)}U_L$  is satisfied, while in the strong anisotropy limit where  $\vec{M}_a \cdot \vec{M}_b = 0$  and  $|\vec{M}_a| = |\vec{M}_b|$  hold,  $V_L = U_L/4$  is satisfied. At the Gaussian fixed point, the behavior of the finite system is governed by the zero-mode<sup>13</sup>, therefore the Gaussian fixed point lies on the  $C_L = 0$  plane. The RG flow on the critical plane, projected onto the  $U_L$ - $V_L$  plane, is shown in Fig. 4 for (a)  $N < N_c$  and (b)  $N > N_c$  cases. In both cases, the RG flow along the (approximately) horizontal direction rapidly converges, while along the (approximately) vertical direction the flow is expected to slowly converge/diverge.

To obtain the RG flow on the critical plane, one must define the critical temperature  $K_c$  for each set of parameters  $A$  and  $\lambda$ . In the present work, we use size-dependent critical temperature  $K_c$  defined as follows: For a given value of  $\lambda$ ,  $A$  and two different system sizes  $L_1 < L_2$ ,  $K_c$  is defined as that at which  $C_{L_1}(K_c) = C_{L_2}(K_c)$  is satisfied. Then one draw a line from  $(U_{L_1}(K_c), V_{L_1}(K_c))$  to  $(U_{L_2}(K_c), V_{L_2}(K_c))$  for various values of  $A$  and  $\lambda$ , then the RG flow diagram shown in Fig. 4 is obtained. It should be noted that the above definition of  $K_c$  induces systematic deviation. For example, consider the RG flow of the isotropic  $\phi^4$  model (set  $v = 0$  in (2)). The flow of  $(U_L, C_L)$  near the Wilson-Fisher fixed point is depicted in Fig. 5 (a)<sup>13</sup>. If one define  $K_c$  by  $C_{L_1}(K_c) = C_{L_2}(K_c)$ , the flow of  $U_L(K_c)$  becomes the one shown in Fig. 5(b), thus the arrow tends to "overshoot" the RG fixed point. However, the direction of the flow can be correctly estimated, and the systematic error vanishes as one approaches the fixed point.

## B. STA models

We also observe the RG flow of the following STA model:

$$H = -K \sum_{\langle ij \rangle} J_{ij} \vec{S}_i \cdot \vec{S}_j, \quad (7)$$

where  $\vec{S}_i$  denotes two-component (XY) or three-component (Heisenberg) vector with  $|\vec{S}_i| = 1$  defined on the lattice site  $i$  of the stacked triangular lattice. We set  $J_{ij} = -1$  (antiferromagnetic) for intra-plane nearest neighbor pairs,  $J_{ij} = 3/4$  (ferromagnetic) for inter-plane nearest neighbor pairs, and otherwise  $J_{ij} = 0$ , so that the Fourier transform of  $J_{ij}$  near the antiferromagnetic mode<sup>14</sup>  $\vec{k}_{AF} = (2\pi/3, 0, 0)$  becomes isotropic in the  $\vec{k}$ -space, i.e.  $J(\vec{k}_{AF} + \vec{k}) \sim J(\vec{k}_{AF}) + c|\vec{k}|^2 + O(|\vec{k}|^4)$ . Note that the critical values of quantities such as  $U_L$ ,  $V_L$ , and  $C_L$  do not depend on the microscopic lattice structure, but *do* depend on the macroscopic lattice structure such as boundary conditions and aspect ratios<sup>15,16</sup>. Therefore we use rectangular system which contains  $L_x \times L_y \times L_z$  spins (see Fig. 6), imposing periodic boundary condition for all three directions. The aspect ratio then becomes  $L_x : \sqrt{3}L_y/2 : L_z$ . We simulated the system with  $(L_x, L_y, L_z) = (21, 24, 21), (42, 48, 42)$ , and  $(84, 96, 84)$  which gives aspect ratio 1 : 0.99 : 1.

The order parameter is defined as follows<sup>6</sup>:

$$\vec{M}_a = \text{Re}[\vec{S}(\vec{k}_{AF})] = \vec{M}_A - \frac{1}{2}\vec{M}_B - \frac{1}{2}\vec{M}_C, \quad (8)$$

$$\vec{M}_b = \text{Im}[\vec{S}(\vec{k}_{AF})] = \frac{\sqrt{3}}{2}\vec{M}_B - \frac{\sqrt{3}}{2}\vec{M}_C, \quad (9)$$

where  $\vec{S}(\vec{k}_{AF})$  denotes Fourier component of  $\vec{S}_i$  at  $\vec{k}_{AF}$ , and  $\vec{M}_A, \vec{M}_B, \vec{M}_C$  denote the magnetization on the three sublattices. Then  $U_L$  and  $V_L$  are calculated from Eq. (5) and Eq. (6).  $C_L$  is calculated as follows:

$$C_L = \frac{\langle |\vec{S}(\vec{k}_{AF} + \vec{k}_1)|^2 + |\vec{S}(\vec{k}_{AF} - \vec{k}_1)|^2 \rangle}{\langle \vec{S}^2(0) \rangle}, \quad (10)$$

where  $\vec{k}_1$  is the smallest, non-zero momentum in the  $\vec{k}$ -space. We observed the values of  $C_L$  for three kinds of direction, namely,  $\vec{k}_1 = (\frac{2\pi}{L_x}, 0, 0)$ ,  $(0, \frac{4\pi}{\sqrt{3}L_y}, 0)$ , and  $(0, 0, \frac{2\pi}{L_z})$ , and confirmed that they coincide each other within statistical errors. This indicates that the simulated system is isotropic.

### III. MONTE CARLO SIMULATION

#### A. chiral $\phi^4$ models

We use single-spin update Metropolis algorithm, since there are no spin reflection axis which preserves the anisotropy term in (2), therefore the cluster algorithm<sup>17</sup> cannot be applied. In a single-spin update process, the new spin value is selected as follows:

$$\vec{\phi}_{new}(i) = \vec{\phi}_{old}(i) + R_g \vec{G} \quad (11)$$

where  $\vec{G}$  is an  $2N$ -component vector, each component being independent Gaussian random variables whose average is 0 and variance is 1.  $R_g$  is the amplitude of random variables, whose optimum value is determined by simulating small systems to minimize the autocorrelation. The optimum values varies from 0.08 to 0.15, depending on the values of  $N$ ,  $A$ , and  $\lambda$ . Each Metropolis sweep is followed by one overrelaxation-type update<sup>18</sup>. Hereafter we refer one Metropolis sweep plus one overrelaxation-type sweep as “MCS”.

For most values of  $A$  and  $\lambda$ , observation is done for every  $2 \times L^2$  MCS, and the autocorrelations of all the successively observed quantities are less than 0.70. When the relaxation is harder, the interval is increased until the aforementioned condition is satisfied. For each values of  $L$ ,  $N$ ,  $A$ , and  $\lambda$ , observations are done from  $10^4$  to  $10^5$  times, depending on the accuracy required to observe the RG flow. Statistical errors are estimated from the Jackknife method. Histogram method<sup>19</sup> is used to calculate thermal averages at  $K$  slightly away from that at which the simulation is actually carried out.

Simulations are mainly carried out on Fujitsu VPP5000 vector processors at JAERI. The checkerboard-wise decomposition of the lattice is used for vectorization. Furthermore, we simultaneously simulate a number of independent systems, whose spins are stored into one long vector. This promotes the vectorization, especially when  $L$  is small, and accelerates the calculations. For  $N = 8$  and  $L = 16$  system, one MCS take 0.84 ms on the VPP5000.

## B. STA models

In this model, the cluster update is not applicable, too. Therefore we use Metropolis update, followed by an overrelaxation sweep, i.e. 180 degree rotation of spin  $\vec{S}_i$  with respect to its local field  $\sum_j J_{ij} \vec{S}_j$ . In the Metropolis update, the new spin direction is chosen as

$$S_x = \sqrt{1 - z^2} \cos(\theta), \quad S_y = \sqrt{1 - z^2} \sin(\theta), \quad S_z = z \quad (12)$$

for Heisenberg case and

$$S_x = \cos(\theta), \quad S_y = \sin(\theta) \quad (13)$$

for XY case, where  $z$  and  $\theta$  are uniformly distributed random number in the range  $[-1, 1)$  and  $[0, 2\pi)$ , respectively. Observation is done for every  $L_x \times L_y/20$  MCS for Heisenberg case and  $L_x \times L_y/10$  MCS for XY case. In these intervals, autocorrelations of the successive observation become less than 0.7 for all system sizes. For the largest system size  $(L_x, L_y, L_z) = (84, 96, 84)$ , observations are done  $0.5 \times 10^4$  times, and  $10^4$  times for other sizes. For  $N = 3$  and  $(L_x, L_y, L_z) = (84, 96, 84)$  system, one MCS takes 27 ms on the VPP5000.

## C. Stiefel's $V_{N,2}$ models

Stiefel's  $V_{N,2}$  model<sup>5</sup> correspond to the Hamiltonian (2) with  $\lambda = \infty$  and  $A = \infty$ , in which restrictions  $\phi_a \cdot \phi_b = 0$ ,  $\phi_a^2 = \phi_b^2 = 1/2$  are imposed to all the spins. We also simulate this model and investigate the RG flow. In the Monte Carlo simulation, only the Metropolis

update is used. Since the  $V_{2,2}$  model is known to exhibit strong first-order behavior<sup>5</sup>, we only simulated the  $V_{3,2}$  model. In this model, the new spin value is selected as follows:

$$\vec{\phi}_a = (z, \sqrt{1-z^2} \cos \theta_1, \sqrt{1-z^2} \sin \theta_1) / \sqrt{2}, \quad (14)$$

$$\vec{\phi}_b = (\sqrt{1-z^2} \sin \theta_2, -\sin \theta_1 \cos \theta_2 - z \cos \theta_1 \sin \theta_2, \cos \theta_1 \cos \theta_2 - z \sin \theta_1 \sin \theta_2) / \sqrt{2} \quad (15)$$

where  $z$  and  $\theta_{1,2}$  are uniformly distributed random number in the range  $[-1, 1]$  and  $[0, 2\pi)$ , respectively. Observation is done for every  $L^2$  Metropolis sweeps and autocorrelations of the successive observation is less than 0.7 for all system sizes. Observation is done  $10^4$  times for all system sizes. One Metropolis sweep of the  $L = 48$  system takes 12.4 ms on the VPP5000.

## IV. RESULTS

### A. XY case

Figure 7 shows the histogram of energy per spin,  $-\sum J_{ij} \vec{S}_i \cdot \vec{S}_j / L_x L_y L_z$ , of  $(L_x, L_y, L_z) = (84, 96, 84)$  case at  $K = 0.7725$ . The double peak of the histogram is a clear evidence of first-order transition. This peak does not appear when the size is smaller, therefore the double peak has not been observed in the past studies of STA-XY model in which smaller systems is used. Note that the first-order behavior has already been observed in the Monte Carlo simulations of other models which possess the same symmetry as the STA-XY model, such as Stiefel model and restricted STA model<sup>20</sup>. These models have stronger anisotropy than the STA-XY model and the first-order behavior can be observed in smaller systems.

Figure 8 shows the RG flow of  $(U_L, V_L)$  at the strong anisotropy region of the  $N = 2$  chiral  $\phi^4$  model and the STA-XY model. One can see that the STA-XY model is on the “runaway” trajectory, which is another evidence of first-order transition. Figure 9 shows the RG flow at the weak anisotropy region, which shows that there are no fixed points other than the  $O(4)$  symmetric one. This means that any models or materials which possess the same symmetry as STA-XY model, namely  $Z_3 \times O(2)$ , exhibits first-order transition.

Fig. 10 shows the vertical velocity of the RG flow, namely  $V_{2L} - V_L$ , plotted against  $V_L$ . If there were fixed point other than the  $O(4)$  symmetric one, this quantity should cross the  $V_{2L} - V_L = 0$  line at the fixed point, but it never occur in this case. The plots for the two different sizes  $L = 6$  and  $L = 8$  coincide within statistical errors, indicating that the system size is large enough to eliminate finite-size artifact of the flow. Moreover, the plot of the chiral  $\phi^4$  model and the STA-XY model are essentially the same. This means that the critical behavior if the STA-XY model is well reproduced by the chiral  $\phi^4$  model.

### B. Heisenberg case

Unlike the STA-XY case, neither the STA-Heisenberg model nor the  $V_{3,2}$  model show the double-peak behavior within the simulated size,  $(L_x, L_y, L_z) = (84, 96, 84)$  for STA-Heisenberg model and  $L = 48$  for  $V_{3,2}$  model.

Figure 11 shows the RG flow of  $(U_L, V_L)$  of the  $N = 3$  chiral  $\phi^4$  model, together with the flow of the STA-Heisenberg model and the  $V_{3,2}$  model. The flow indicates that the

STA-Heisenberg model and  $V_{3,2}$  model are on the “runaway” trajectory, therefore undergoes first-order transition. Figure 12 shows the RG flow at the weak anisotropy region. The vertical component of the flow is always positive and there are no fixed point other than the  $O(6)$  symmetric one. This means that any models or materials which possess the same symmetry as STA-Heisenberg model, namely  $Z_3 \times O(3)$ , exhibits first-order transition.

Fig. 13 shows the vertical velocity of the RG flow  $V_{2L} - V_L$  plotted against  $V_L$ . In this case, this quantity not only depends on  $V_L$  but also on  $U_L$ , although the dependence is weak. Therefore the plot is not fitted to a line. However, it seems impossible that the plot has zeroes when the size  $L$  is increased and a stable fixed point emerges. As in the XY case, the plots of the chiral  $\phi^4$  model and the STA-Heisenberg model are essentially the same. This means that the critical behavior if the STA-Heisenberg model is well reproduced by the chiral  $\phi^4$  model.

### C. $N = 8$ case

It is necessary to demonstrate that the MCRG scheme presented in Sec. II is able to detect the chiral fixed point if it does exist. For this purpose, we investigated  $N = 8$  case, which is greater than any theoretical estimate of  $N_c$  in literature<sup>7–10</sup>. Figure 14 shows the RG flow of  $(U_L, V_L)$  for  $L = 8 \rightarrow 16$ . The stable chiral fixed point  $C_1$  and the unstable chiral fixed point  $C_2$  are clearly seen.

Fig. 15 shows the vertical velocity of the RG flow  $V_{2L} - V_L$  plotted against  $V_L$ , using only the data near the stable fixed point  $C_1$ . Unlike the  $N = 2$  and the  $N = 3$  case, this plot has a zero. The plots of the two different size coincides within statistical error, which indicate that the simulated system is large enough to observe the RG flow.

## V. CONCLUSION

The large scale Monte Carlo simulation of the STA-XY model have revealed that the transition is of first-order. This is the first numerical work to confirm the first-order transition of the simple STA-XY model. We have also investigated the RG flow the  $2N$ -component chiral  $\phi^4$  model numerically and found that there are no chiral fixed point in  $N = 2$  and  $N = 3$  cases, and we conclude that the STA-Heisenberg model also undergoes first-order transition. For  $N = 8$  case, we have found the chiral fixed point, thus the value of  $N_c$  is estimated as  $3 < N_c < 8$ . Further study to determine the precise value of  $N_c$  may be of some interest, because such a study will serve to test the accuracy of field theoretical perturbation techniques. However, once the nature of physical relevant case  $N = 3$  and  $N = 2$  is clarified, the precise value of  $N_c$  is of less importance.

## VI. ACKNOWLEDGMENTS

The present author is grateful to D. Loison, B. Delamotte, and K. B. Varnashev for useful comments.

- <sup>1</sup> M. Tissier, B. Delamotte, and D. Mouhanna, Phys. Rev. Lett.**84**, 5208 (2000); preprint, cond-mat/0107183;cond-mat/0101167.
- <sup>2</sup> A. Pelissetto, P. Rossi and E. Vicari Phys. Rev. B**63** R140414 (2001); Nucl. Phys. B **607**, 605 (2001); preprint, cond-mat/0106525.
- <sup>3</sup> K. B. Varnashev, preprint.
- <sup>4</sup> V. P. Plakhty, J. Kulda, D. Visser, E. V. Moskvina, and J. Wosnitza, Phys. Rev. Lett.**85**, 3942 (2000).
- <sup>5</sup> D. Loison and K. D. Schotte, Euro. Phys. J.B **14**, 125 (2000).
- <sup>6</sup> H. Kawamura, J. Phys.: Condens. Matter **10**, 4707 (1998).
- <sup>7</sup> H. Kawamura, J. Phys. Soc. Jpn.**59**, 2305 (1990).
- <sup>8</sup> S. A. Antonenko, A. I. Sokolov and K. B. Varnashev, Phys. Lett. A **208**, 161 (1995).
- <sup>9</sup> S. A. Antonenko and A. I. Sokolov, Phys. Rev. B**49**, 15901 (1994).
- <sup>10</sup> G. Zumbach, Phys. Rev. Lett.**71**, 2421 (1993); Nucl. Phys. B **413**, 771 (1994).
- <sup>11</sup> H. Kawamura, J. Phys. Soc. Jpn.**61**, 1299 (1992).
- <sup>12</sup> M. L. Plumer and A. Mailhot, Phys. Rev. B **50**, 16113 (1994).
- <sup>13</sup> M. Itakura, Phys. Rev. E**61**, 5924 (2000).
- <sup>14</sup> The first Brillouin zone is an (approximately regular) hexagon in the  $x$ - $y$  plane and  $\vec{k}_{AF}$  is on the vertex of the hexagon.
- <sup>15</sup> K. Kaneda and Y. Okabe, Phys. Rev. Lett. **86**, 2134 (2001).
- <sup>16</sup> K. Kaneda, Y. Okabe, and M. Kikuchi, J. Phys. A **32**, 7263 (1999).
- <sup>17</sup> U. Wolff, Phys. Rev. Lett. **62**, 361 (1989).
- <sup>18</sup> M. Caselle and M. Hasenbusch, J. Phys. A **31**, 4603 (1998).
- <sup>19</sup> A. M. Ferrenberg and R. H. Swendsen, Phys. Rev. Lett. **61**, 2635 (1988).
- <sup>20</sup> D. Loison and K. D. Schotte, Euro. Phys. J.B**5**, 735 (1998).

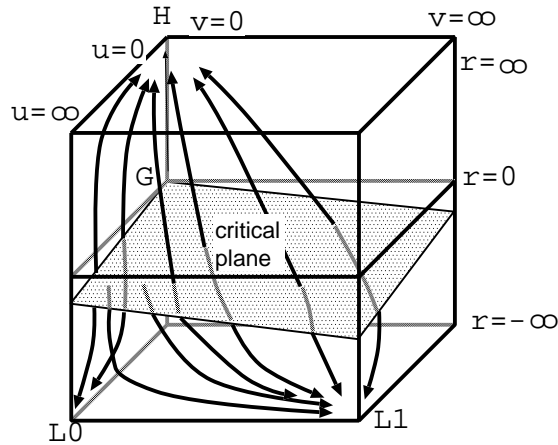


FIG. 1. Renormalization flow of  $r$ ,  $u$ , and  $v$ . H, G, L<sub>0</sub>, and L<sub>1</sub> denote the high-temperature, Gaussian, isotropic low-temperature, and anisotropic low-temperature fixed point, respectively.



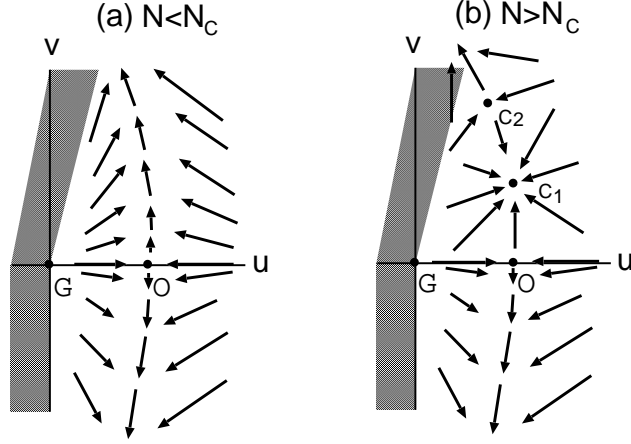


FIG. 2. Renormalization flow on the critical plane projected onto the  $u$ - $v$  plane for (a)  $N < N_c$  and (b)  $N > N_c$ . Shaded area is unstable region. G, O,  $C_1$ , and  $C_2$  denote Gaussian,  $O(2N)$ -isotropic, stable chiral, and unstable chiral fixed points, respectively.

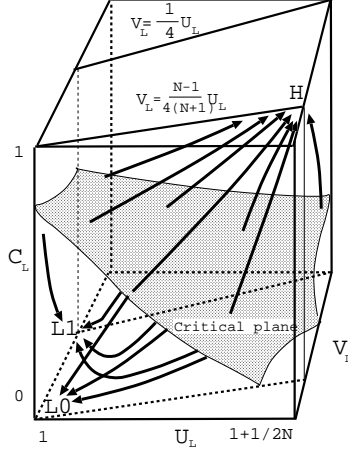


FIG. 3. Renormalization flow of  $C_L$ ,  $U_L$ , and  $V_L$ .

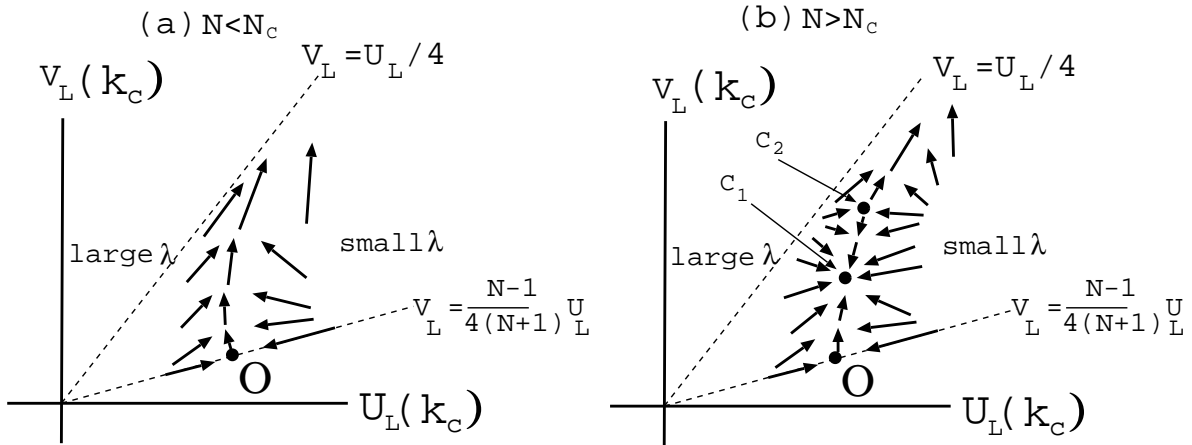


FIG. 4. Renormalization flow on the critical plane projected onto the  $U_L$ - $V_L$  plane for (a)  $N < N_c$  and (b)  $N > N_c$ . O,  $C_1$ , and  $C_2$  denote  $O(2N)$ -isotropic, stable chiral, and unstable chiral fixed point, respectively.

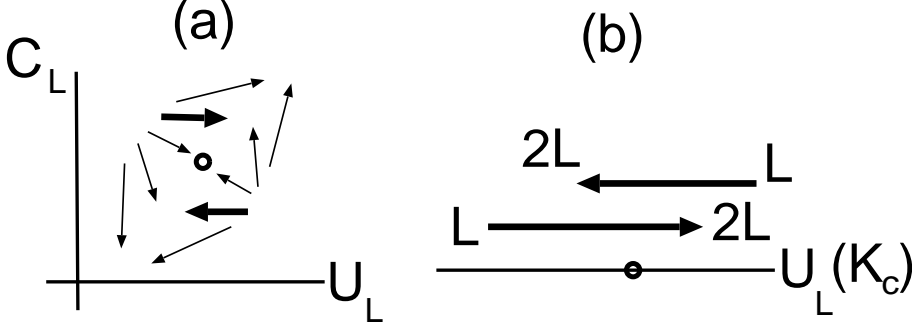


FIG. 5. (a) Renormalization flow of  $C_L$  and  $U_L$  for isotropic model  $v = 0$  near the Wilson-Fisher fixed point. (b) RG flow of  $U_L(K_c)$ . See the main text.

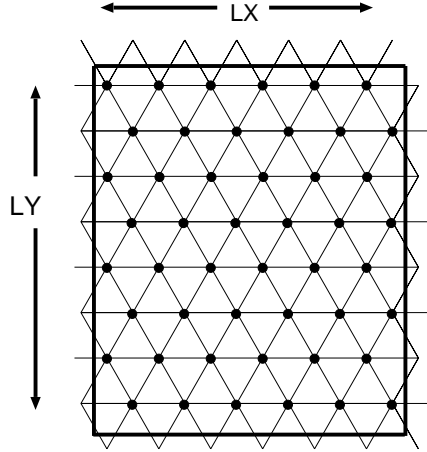


FIG. 6. Rectangular system used for the simulation of stacked triangular antiferromagnet. The figure shows a system with  $L_x = 6$ ,  $L_y = 8$ . This layer is stacked  $L_z$  times.

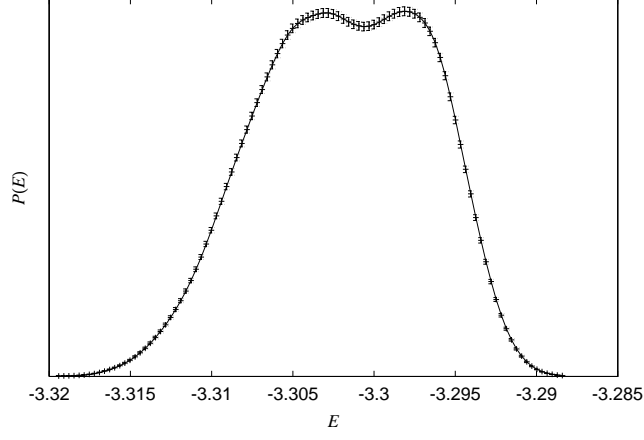


FIG. 7. Histogram of energy per spin for  $(L_x, L_y, L_z) = (84, 96, 84)$  case at  $K = 0.7725$ .

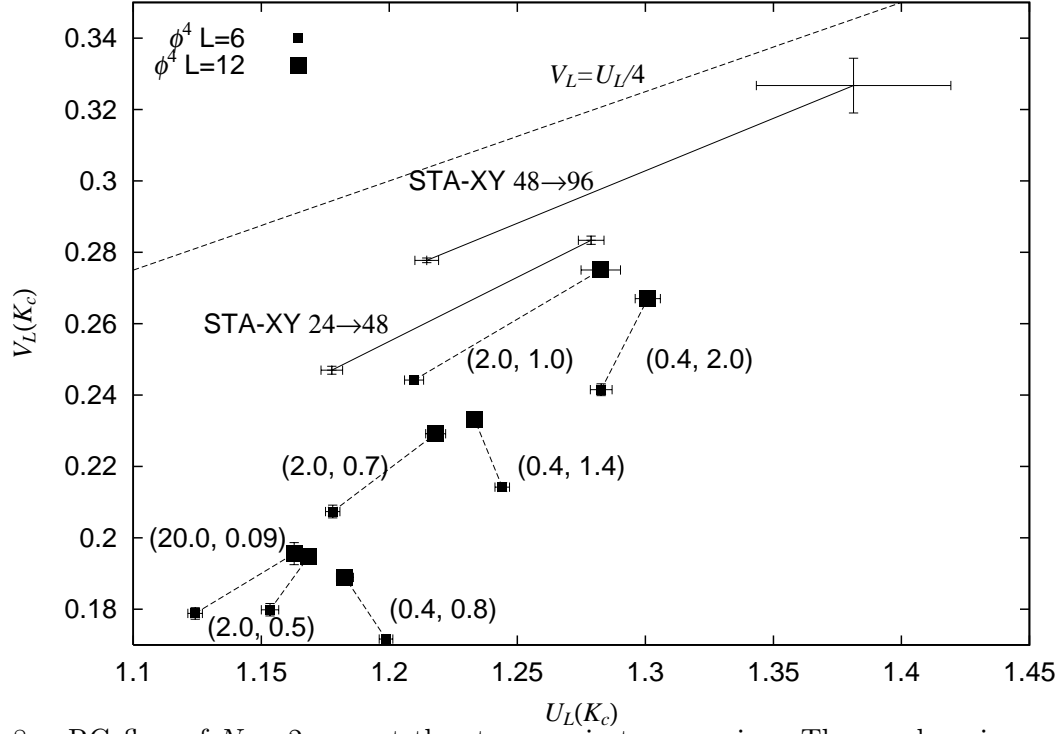


FIG. 8. RG flow of  $N = 2$  case at the strong anisotropy region. The numbers in parenthesis are the values of  $(\lambda, A)$  of the chiral  $\phi^4$  model.

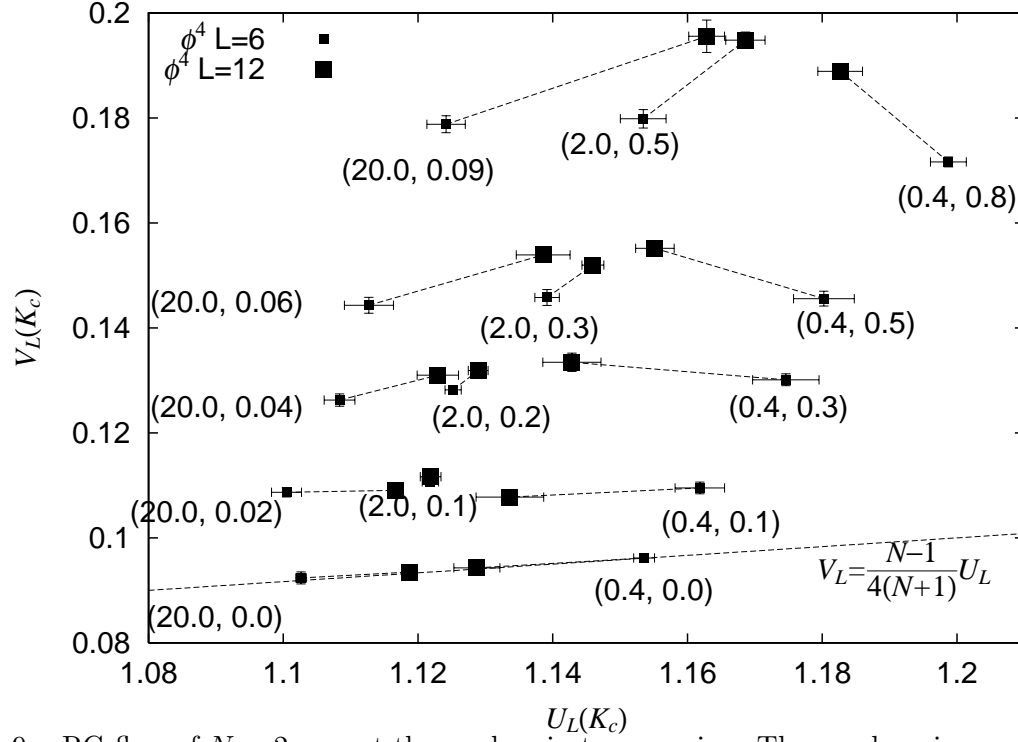


FIG. 9. RG flow of  $N = 2$  case at the weak anisotropy region. The numbers in parenthesis are the values of  $(\lambda, A)$  of the chiral  $\phi^4$  model.

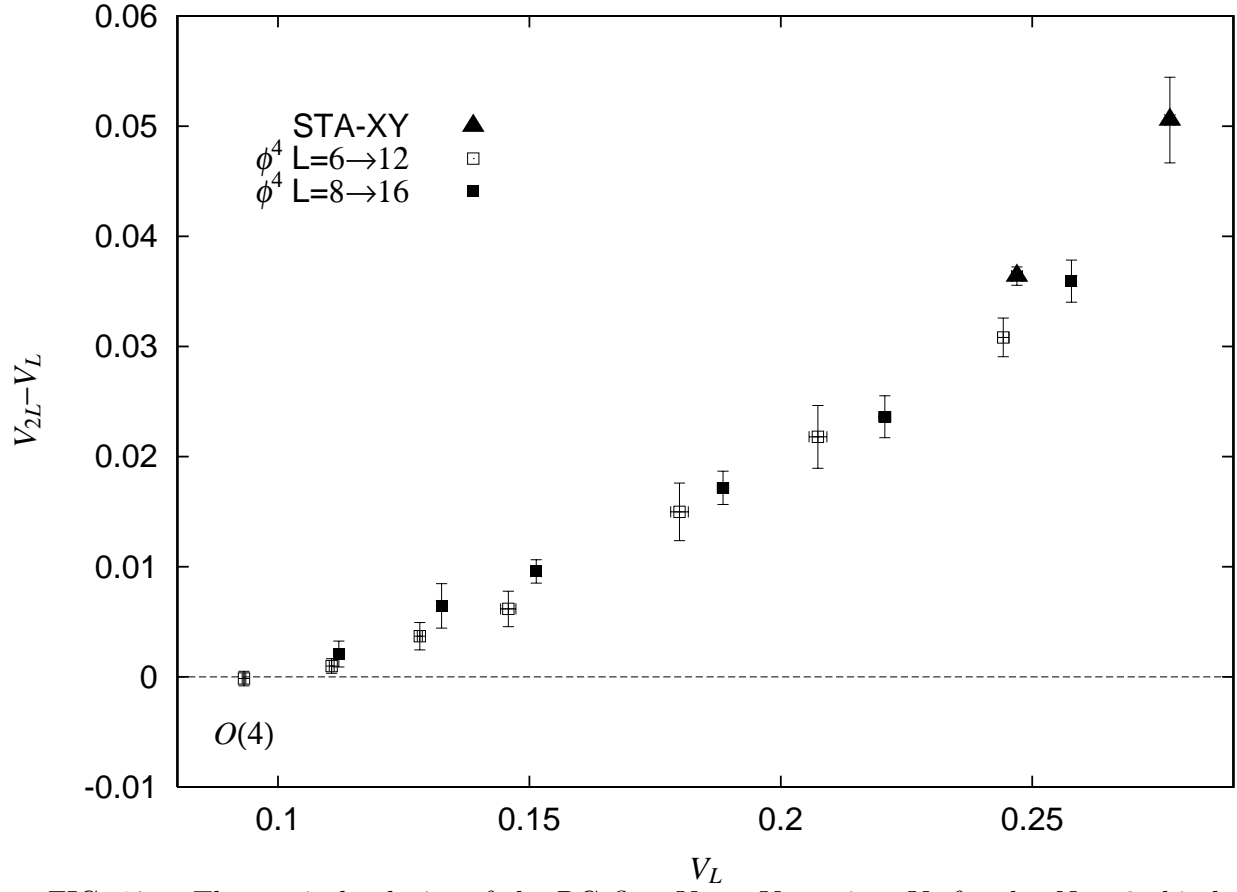


FIG. 10. The vertical velocity of the RG flow  $V_{2L} - V_L$  against  $V_L$  for the  $N = 2$  chiral  $\phi^4$  model and the STA-XY model. “ $O(4)$ ” is the  $O(4)$ -symmetric fixed point.

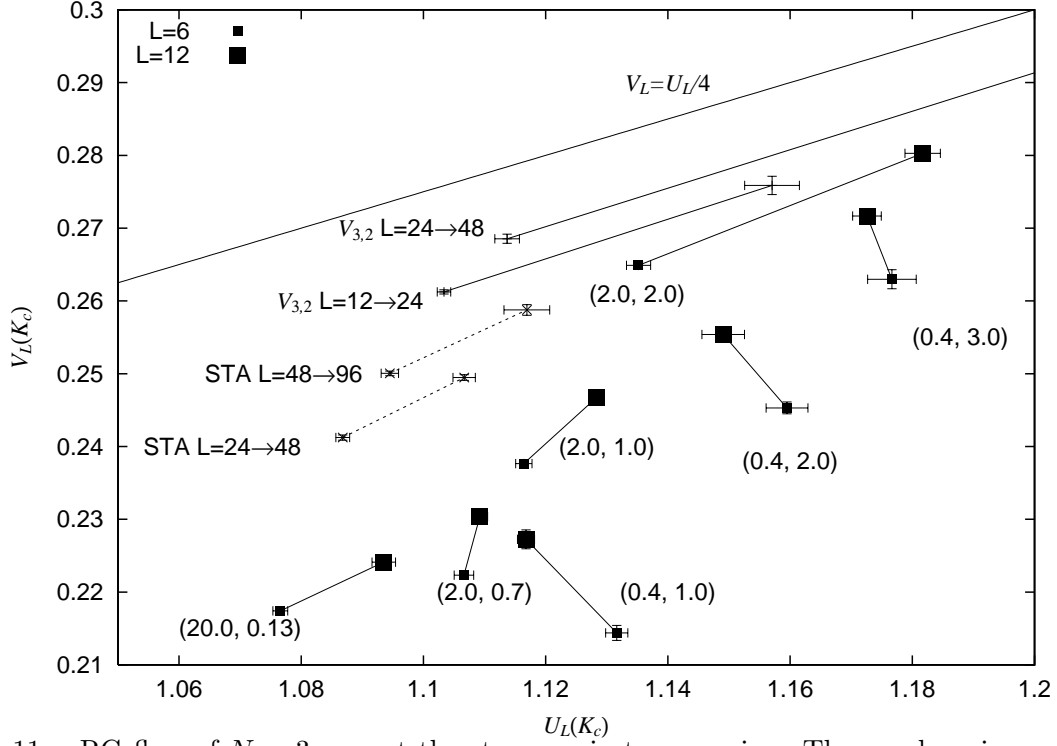


FIG. 11. RG flow of  $N = 3$  case at the strong anisotropy region. The numbers in parenthesis are the values of  $(\lambda, A)$  of the chiral  $\phi^4$  model.

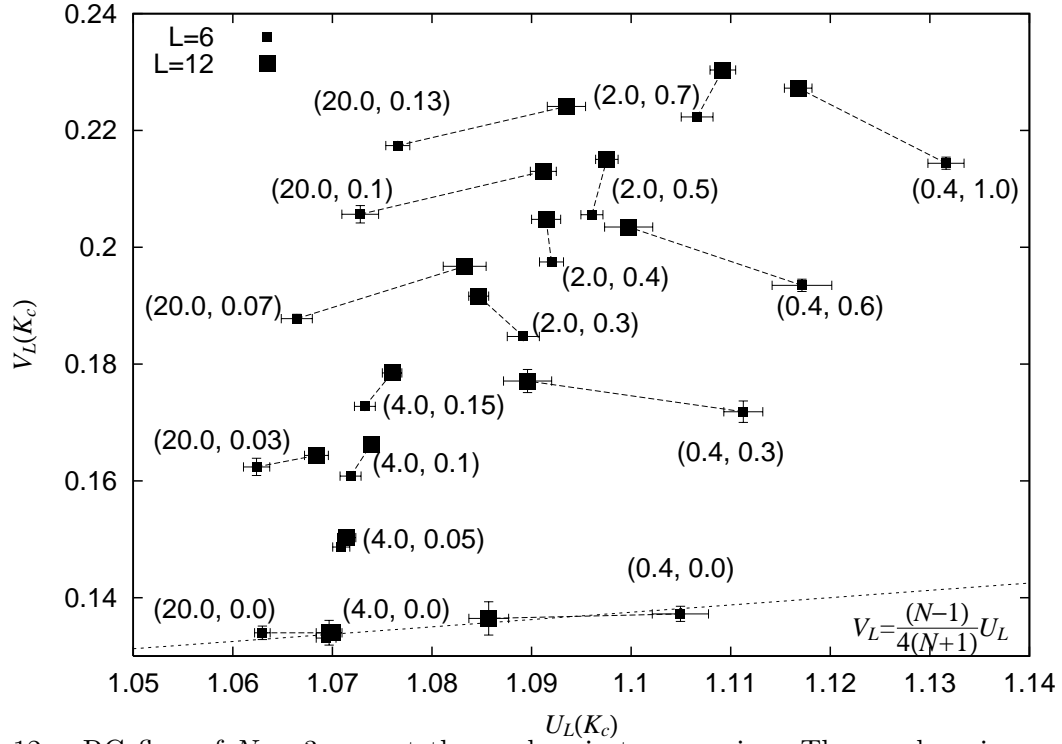


FIG. 12. RG flow of  $N = 3$  case at the weak anisotropy region. The numbers in parenthesis are the values of  $(\lambda, A)$  of the chiral  $\phi^4$  model.

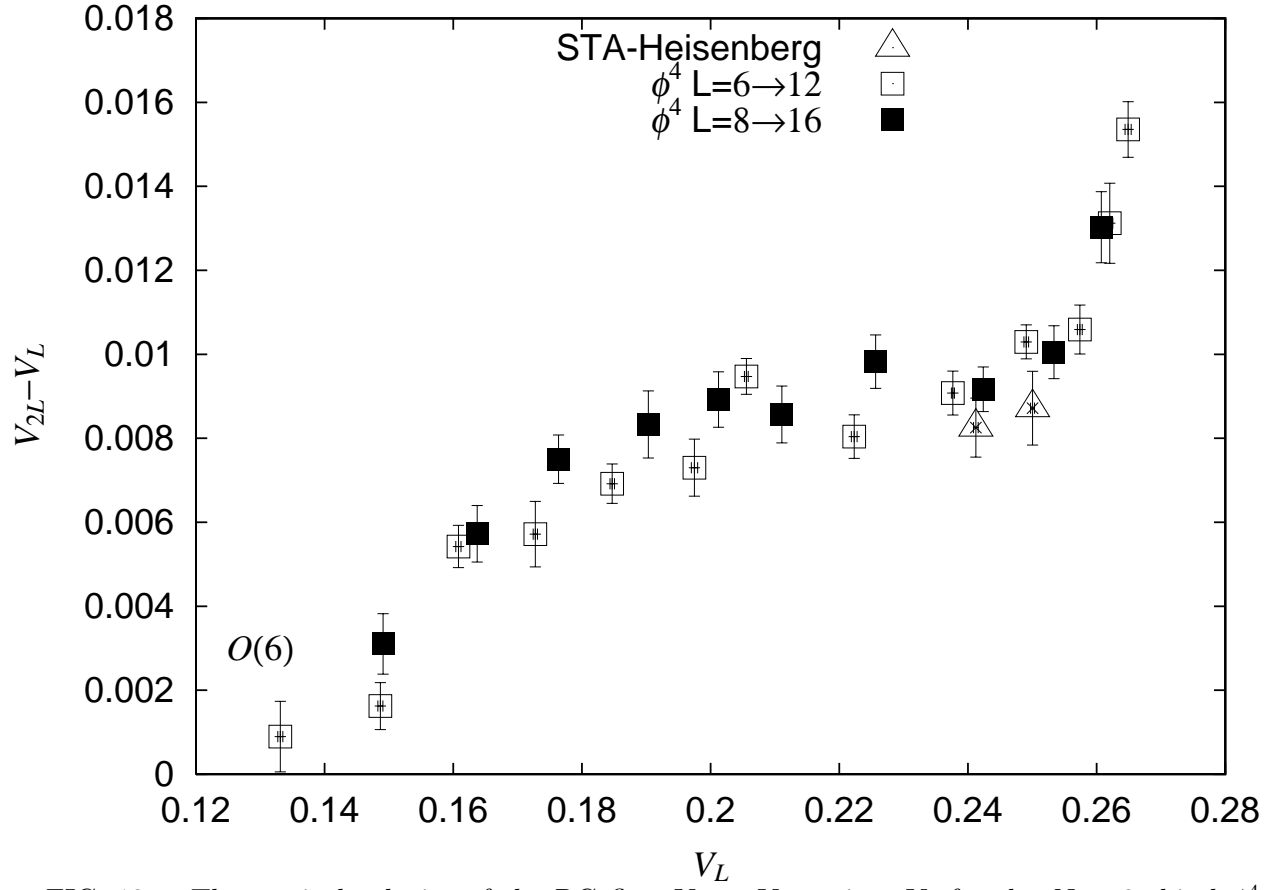


FIG. 13. The vertical velocity of the RG flow  $V_{2L} - V_L$  against  $V_L$  for the  $N = 3$  chiral  $\phi^4$  model and the STA-Heisenberg model. “ $O(6)$ ” is the  $O(6)$ -symmetric fixed point.

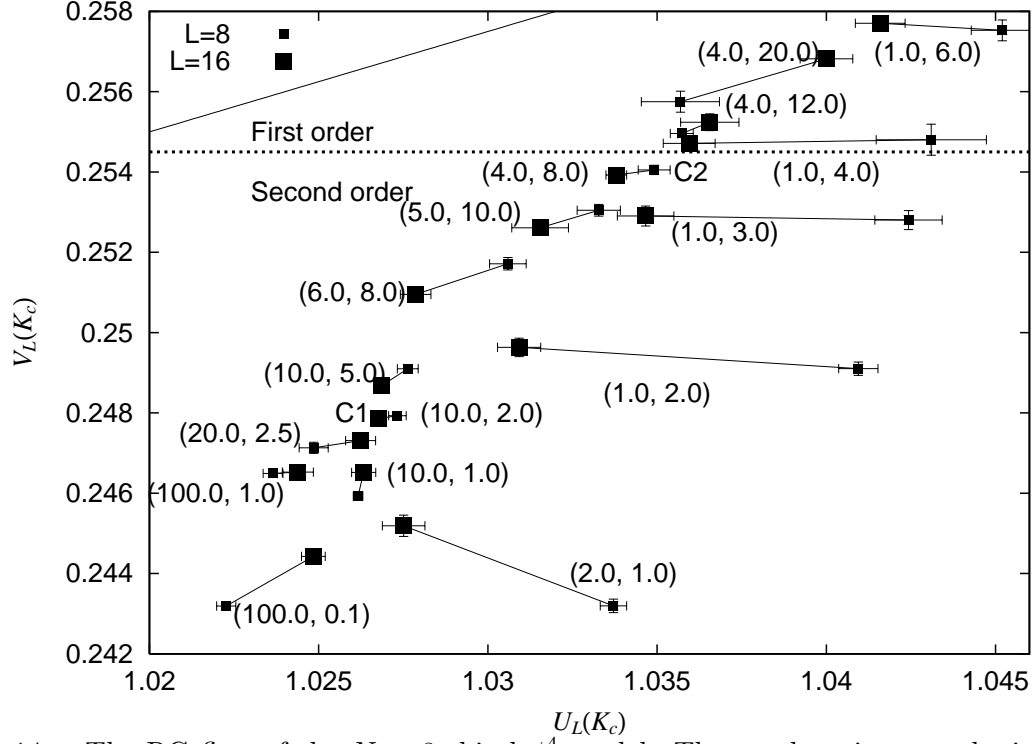


FIG. 14. The RG flow of the  $N = 8$  chiral  $\phi^4$  model. The numbers in parenthesis show the values of  $(\lambda, A)$ . C1 and C2 denote the stable and unstable RG fixed point, respectively.

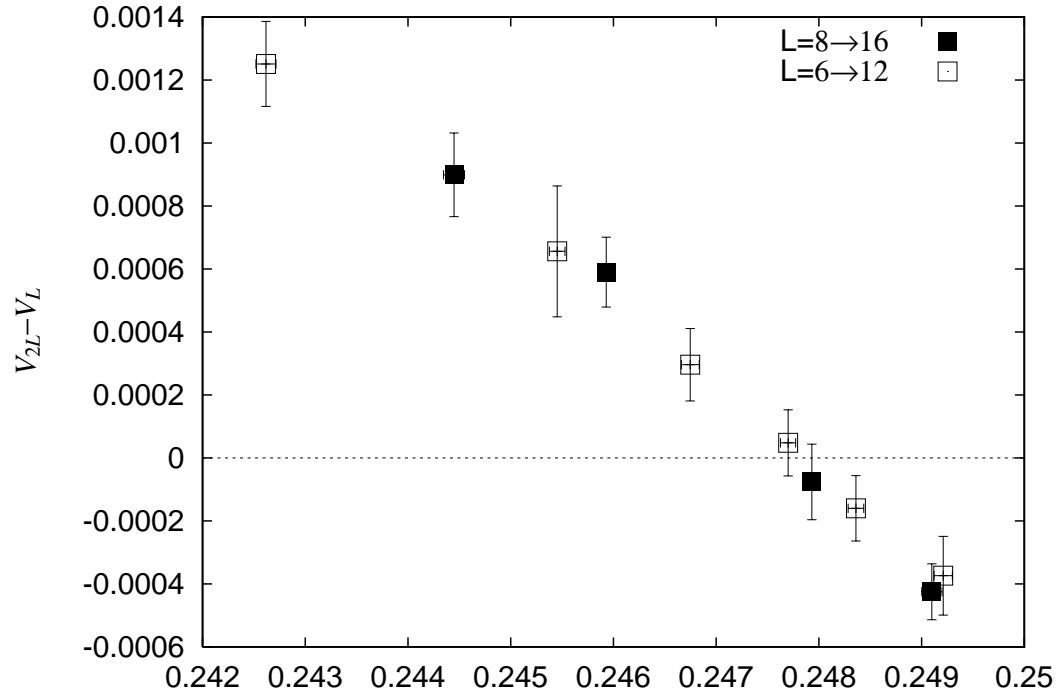


FIG. 15. The vertical velocity of the RG flow  $V_{2L} - V_L$  against  $V_L$  near the stable chiral fixed point of the  $N = 8$  chiral  $\phi^4$  model.